Revista Portuguesa de Estomatologia, Medicina Dentária e Cirurgia Maxilofacial
Portuguese Journal of Stomatology, Dental Medicine and Maxillofacial Surgery
REV PORT ESTOMATOL MED DENT CIR MAXILOFAC. 2026;67(x):1-13

Original Research

Reference-based deviation and repeatability of a complete-arch implant photogrammetry system: an in vitro study

Juliana L. Rainho[1], *Ricardo J. Pinto*[1,2], *Francisco J. Maligno da Silva*[3], *João M. Caramês*[1,2,4], *Duarte S. Marques*[1,2,4,*]

[1] *Faculty of Dental Medicine, University of Lisbon, Lisbon, Portugal*
[2] *Implantology Institute, Lisbon, Portugal*
[3] *Faculty of Dental Medicine, University of Porto, Porto, Portugal*
[4] *Biomedical and Oral Sciences Research Unit (UICOB), LIBPhys-FCT UIDB/04559/2020, Lisbon, Portugal*

ARTICLE INFO

Article history:
Received 24 July 2026
Accepted 4 October 2026
Available online 16 November 2026

Keywords:
Computer-Aided Design
Dental arch
Dental implants
Dental impression technique
Dental prosthesis, implant-supported
Imaging, three-dimensional
Photogrammetry
Reproducibility of results

ABSTRACT

Objectives: To evaluate the reference-based deviation and repeatability of a photogrammetry system (TUPEL 3D) for complete-arch implant acquisition, and the influence of implant number, measurement location, and operator.

Methods: Two configurations of an in vitro mandibular model were used: six implants and four implants, with multiunit abutments. Two operators performed 80 acquisitions (20 per operator/configuration). Linear and angular inter-implant measurements were compared with an industrial scanner reference. Independent- and paired-sample t tests compared configurations, operators, and locations; Holm-adjusted *P* values are reported.

Results: Across all measured pairs, the six-implant configuration showed higher linear and angular deviations (linear root mean square deviation: 94.69 ± 9.27 versus 54.60 ± 4.68 µm; $P < .001$). The six pairs common to both configurations revealed no significant angular differences ($P = .901$) and slight linear mean absolute deviation differences (six versus four implants: 42.82 ± 5.95 versus 39.68 ± 4.48 µm; $P = .038$). Posterior-distal measurements showed greater deviations ($P < .001$). Linear repeatability deviation was higher with six implants (12.52 ± 3.62 versus 9.39 ± 4.15 µm; $P = .003$). Operator-related differences in reference-based metrics were inconsistent across measurement domains.

Conclusions: No statistically significant between-operator differences were detected in repeatability, and repeatability was lower with six implants. Higher deviations in the six-implant configuration were mainly associated with posterior-distal measurement locations rather than with implant number itself. (Rev Port Estomatol Med Dent Cir Maxilofac. 2026;67(x):1-13)

© 2026 Sociedade Portuguesa de Estomatologia e Medicina Dentária. Published by SPEMD. This is an open access article under the CC BY-NC-ND license (http://creativecommons.org/licenses/by-nc-nd/4.0/).

* Corresponding author.
E-mail address: duarte.marques@campus.ul.pt (Duarte Nuno da Silva Marques).
http://doi.org/10.24873/j.rpemd.2026.12.1594
1646-2890/© 2026 Sociedade Portuguesa de Estomatologia e Medicina Dentária. Published by SPEMD.
This is an open access article under the CC BY-NC-ND license (http://creativecommons.org/licenses/by-nc-nd/4.0/).

Introduction

Accurate transfer of implant position is essential to achieve passive fit, which is associated with fewer mechanical and biological complications and improved long-term outcomes.[1–7] Inaccuracies in implant position recording may result in framework misfit and increased stress at the implant–prosthesis interface – a phenomenon that is particularly relevant in complete-arch prostheses, where multiple implants are connected by rigid frameworks and even small positional discrepancies may contribute to mechanical complications such as screw loosening or fracture, as well as biological consequences including marginal bone loss.[1,3,7,8] Therefore, high accuracy in implant position acquisition remains a fundamental requirement in complete-arch implant prosthodontics.

The transition from conventional impression techniques to digital workflows in implant prosthodontics has been associated with enhanced efficiency, better patient-reported outcomes, and simplified digital model storage.[4,8–10] Intraoral scanning and photogrammetry have been investigated as digital approaches to complete-arch implant acquisition, with performance varying across systems and acquisition workflows.[3,4,9,11]

Although intraoral scanning has transformed digital dentistry, complete-arch implant acquisition is particularly demanding. Due to the progressive propagation of stitching-related deviations that make the acquisition process more susceptible to error accumulation, scanning accuracy decreases as arch span increases.[8,12,13] Thus, recording complete-arch implant positions remains challenging, particularly in edentulous scenarios, due to long scanning distances, limited anatomical landmarks, and the need for image stitching, which may compromise the accuracy and reliability of the final digital record.[2–5,8,11–13] These limitations have been consistently reported in both in vitro and clinical investigations of complete-arch implant impressions.[3,8,12,13]

Photogrammetry-based systems have been introduced to overcome some of these limitations by capturing implant positions using optical markers and device-specific recognition protocols, thereby reducing reliance on sequential image stitching and potentially minimizing distortion in complete-arch workflows.[2,4,9] Several recent clinical and laboratory studies, as well as systematic reviews, suggest that photogrammetry may provide improved trueness and precision compared with intraoral scanning in complete-arch implant acquisition.[2,4,5,9,10] However, performance appears to depend heavily on the specific device, acquisition protocol, and data processing workflow. Thus, each newly introduced system requires independent validation.[10,14] In addition, emerging evidence suggests that factors such as implant number and spatial distribution may influence the magnitude of deviation, although these variables have not been consistently evaluated across studies.[12,15]

Despite the increasing adoption of photogrammetry in implant dentistry, the rapid introduction of new commercial systems has outpaced the availability of independent scientific validation. Consequently, findings from one system should not be directly extrapolated to others, highlighting the need for system-specific evaluation of measurement performance and clinical reliability. The present study was designed to address this need by evaluating a recently introduced photogrammetry system using a previously validated master model framework for direct comparison with an established reference dataset, while focusing on acquisition-level performance metrics derived from linear and angular measurements. To the best of the authors' knowledge, no independent data on this system have been previously reported.

The primary objective of this study was to evaluate the reference-based deviation and repeatability of a photogrammetry system in complete-arch implant acquisition using a reference dataset derived from an industrial optical scanning system. The secondary objective was to evaluate how operator-related factors, implant number, and measurement location affect deviation magnitude. The null hypotheses were that the performance of the photogrammetry system would not differ between four-implant and six-implant configurations; operator-related factors would not influence deviation magnitude; and measurement location would not influence deviation magnitude.

Material and Methods

An in vitro study was conducted to evaluate the performance of the TUPEL photogrammetry system (TUPEL 3D Dental Implant Scanner, software version 2.1.3; Tupel Ltd, Oxford, UK) for complete-arch implant position acquisition in a laboratory setting. The ATOS industrial optical scanning system (ATOS Compact Scan 12M, GOM GmbH, Braunschweig, Germany) was used as the reference standard. A comparative design was adopted to assess how implant configuration, operator, and intra-arch measurement location affected deviation magnitude. All TUPEL acquisitions, data processing, statistical analyses, and comparisons reported in this study were performed specifically for this investigation.

The master model was an edentulous mandibular resin model with simulated pink silicone gingiva (4010G; Demobone), rehabilitated with six implants (Bone Level Tapered Implant; Institut Straumann AG, Basel, Switzerland) and multi-unit abutments (SRA RC screw-retained abutment; Institut Straumann AG), tightened according to the manufacturer's recommendations. The implants were located at FDI tooth positions 36, 34, 32, 42, 44, and 46. The six-implant configuration included all six implant positions. The four-implant configuration comprised the implants at positions 34, 32, 42, and 44, with the scan bodies at positions 36 and 46 physically removed from the model for acquisitions. The four selected implants resulted in six inter-implant pairs (34–32, 34–42, 34–44, 32–42, 32–44, and 42–44), common to both configurations.

The reference dataset, comprising linear and angular measurements, was derived from industrial optical scans of the master model previously generated by our research group.[4] These scans included six acquisitions for the four-implant configuration and six acquisitions for the six-implant configuration that were reused exclusively to establish the high-accuracy reference standard for this investigation. Polyetheretherketone (PEEK) scan bodies (Straumann CARES Mono; Institut Straumann AG, Basel, Switzerland) were used for all

reference acquisitions, following the manufacturer's instructions. ATOS was selected as the reference because of its high measurement accuracy and widespread application in industrial dimensional analysis. This scanner and acquisition protocol had been previously validated for this experimental setup and showed intra-scanner variability below 3 µm.[4] For each implant configuration, the reference dataset was established by averaging the corresponding measurements across the six acquisitions, reducing measurement variability and providing a stable basis for comparison.

According to ISO 5725-1, measurement accuracy encompasses both trueness and precision, with precision describing the closeness of agreement between independent measurement results under specified conditions.[16] In the present study, as the reference was obtained using a high-accuracy comparison system rather than a certified nominal geometry, the reported reference-based metrics express deviation relative to this reference standard rather than absolute trueness in the strict metrological sense. Accordingly, measurements derived from comparisons with the ATOS-based reference dataset are described throughout this study as reference-based deviations. Repeatability was assessed separately to characterize within-operator variability across repeated acquisitions. Because the reference and test datasets were reconstructed using different scan bodies and library-based procedures, the observed deviations cannot be attributed exclusively to the TUPEL acquisition workflow.

An a priori sample size calculation (two-sided independent-samples *t* test; α = 0.05; power = 80%) used data from a previous study by the present research group with the same master model, measurement protocol, and 20 acquisitions per condition.[17] The four- versus six-implant angular differences of the two dedicated photogrammetry devices with the lowest discrepancies (iCam, 0.20 ± 0.11° versus 0.33 ± 0.18°; PIC, 0.22 ± 0.13° versus 0.38 ± 0.22°) and the linear difference between these devices (35.76 ± 25.40 versus 72.23 ± 54.71 µm, four implants) corresponded to standardized effect sizes (*d*) of 0.86 to 0.89. Assuming $d = 0.91$, 20 acquisitions per subgroup provide 80% power (75% to 78% for $d = 0.86$ to 0.89), which determined our required sample size.

Implant position acquisition was performed using the TUPEL photogrammetry system with manufacturer-specific metallic scan bodies (Tupel Ltd) used for all acquisitions (Figures 1 and 2). Two operators performed acquisitions in two implant configurations: four-implant and six-implant. For each operator and configuration, 25 scans were initially performed, resulting in 100 acquisitions overall. The first five scans from each operator/configuration combination were excluded as part of an initial familiarization phase. The remaining 20 scans per operator/configuration combination were retained for statistical analysis, resulting in a final analytical dataset of 80 acquisitions. The acquisition order was fixed and not randomized. Operator A first completed all acquisitions for the six-implant configuration, followed by the four-implant configuration. Subsequently, Operator B performed the acquisitions in the same sequence. Each operator completed all acquisitions for both configurations within a single session. Neither operator had prior experience with the TUPEL system; however, Operator B had previous clinical experience with other photogrammetry-based implant acquisition systems.



Figure 1. TUPEL 3D Dental Implant Scanner (Tupel Ltd, Oxford, UK) used for photogrammetry-based implant position acquisition.

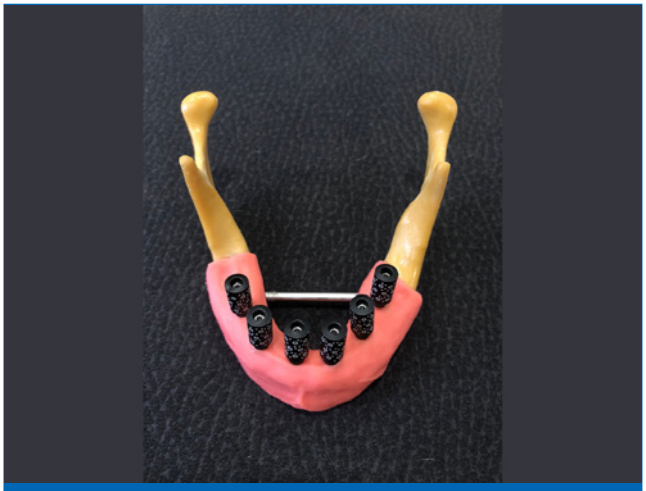


Figure 2. Edentulous mandibular master model showing the six-implant configuration with multiunit abutments and manufacturer-specific metallic scan bodies used for photogrammetry acquisitions.

The TUPEL system was calibrated prior to data acquisition following the manufacturer's protocol, and no additional calibration was required during acquisition. The acquisition protocol followed the manufacturer's instructions, which allow two alternative methods for scan body seating. Operator A tightened the scan bodies using a calibrated prosthetic dynamometric screwdriver (Torq Control®, Anthogyr, Sallanches, France) set to 10 N·cm, whereas Operator B performed manual finger-tightening.[18] These two distinct but manufacturer-sanctioned methods aimed to evaluate the system's performance under different clinical tightening protocols. All acquisitions were performed in the same laboratory setting following the manufacturer's instructions. Ambient lighting conditions remained stable throughout the acquisition process, with no direct light interference. The acquisition distance complied with the manufacturer's recommended operating range.

The TUPEL system allows the integration of user-defined implant libraries. In this study, a standardized stereolithography file corresponding to the implant analog geometry (SRA RC; Institut Straumann AG) was provided to the manufacturer

and adapted for system compatibility. The TUPEL system enabled direct export of implant-level datasets using the selected implant library, without requiring additional CAD-based scan body recognition procedures. In contrast, for the reference dataset, scan body recognition and implant reconstruction had been performed using dental CAD software (exocad; exocad GmbH, Darmstadt, Germany). In both workflows, implant replicas were defined using the same implant analog geometry, thereby standardizing the underlying implant analog definition across datasets.

All datasets were imported into reverse engineering software (Geomagic Control X; 3D Systems, Rock Hill, SC, USA) for quantitative analysis. Linear and angular measurements were performed following a standardized measurement protocol similar to those previously described for implant position accuracy assessment.[19] For each implant, a reference circle was defined from three points selected at the base of the implant analog connection. The center of this circle served as the implant reference point, and a vector passing through this point and perpendicular to the plane of the circle represented the implant axis. Linear measurements were defined as the distances between the reference points of each implant pair, and angular measurements as the angles between their corresponding implant axes (Figure 3). The same measurement protocol was applied to both the reference and test datasets to ensure comparability.

Measurements of the TUPEL datasets were performed by Operator A, whereas measurements of the ATOS reference datasets were performed by Operator B. This resulted in six linear and six angular measurements for the four-implant configuration, and 15 linear and 15 angular measurements for the six-implant configuration. The acquisition was defined as the primary inferential unit, with all variables within each acquisition summarized into single outcome metrics for statistical analysis.

Reference-based deviation and repeatability metrics were operationalized at the acquisition level. Mean absolute deviation from the configuration-specific reference values (MADref) was calculated. The reference values (r_j) were defined as the mean of repeated ATOS measurements for each corresponding linear or angular variable. Accordingly, MADref was calculated as:

$$MADref_i = (1/p) \Sigma |x_{ij} - r_j|,$$

where x_{ij} is the value of variable j in acquisition i, r_j is the corresponding reference value, and p is the number of variables in that configuration.

Overall deviation from the reference values was quantified as the root mean square deviation from the same reference values (RMSref), calculated as:

$$RMSref_i = \sqrt{((1/p) \Sigma (x_{ij} - r_j)^2)}.$$

Repeatability was quantified as the root mean square deviation from the operator-specific mean values (RMSrep). The operator-specific mean values (c_j) were defined as the mean of repeated measurements for each linear or angular variable within each operator and configuration. Accordingly, RMSrep was calculated as:

$$RMSrep_i = \sqrt{((1/p) \Sigma (x_{ij} - c_j)^2)},$$

where x_{ij} is the value of variable j in acquisition i, c_j is the corresponding operator-specific mean value, and p is the number of variables in that configuration.

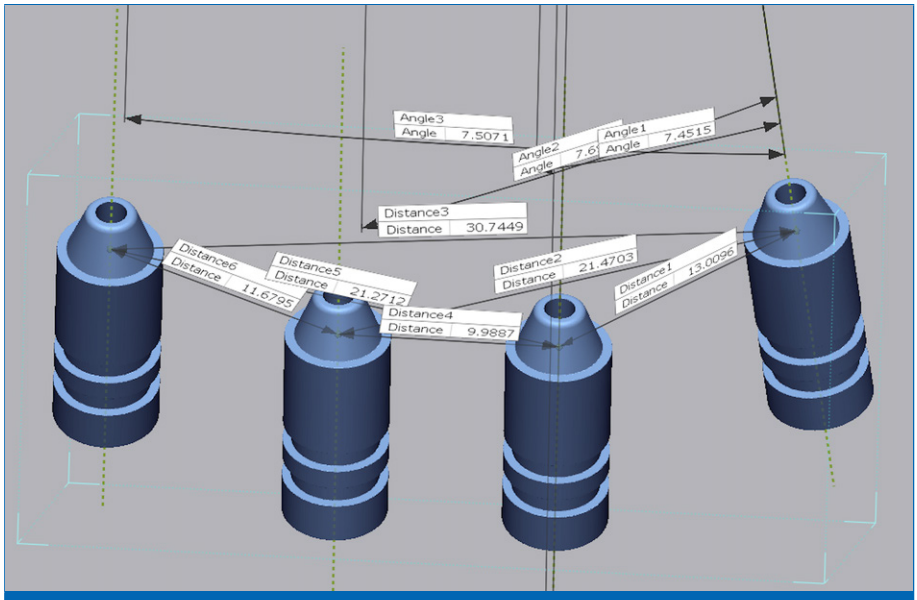


Figure 3. Representative screenshot of the measurement workflow in Geomagic Control X (3D Systems, Rock Hill, SC, USA). Linear measurements were obtained between implant centers, and angular measurements were calculated between the long axes of the implants. The displayed distance values are in millimeters (mm), and the angular values are in degrees (°). Linear deviations in the analyses are reported in micrometers (µm).

For MADref, deviations were converted to absolute values before averaging. For RMSref and RMSrep, deviations were squared before aggregation; therefore, positive and negative deviations could not cancel each other. Consequently, all three acquisition-level summary metrics represent deviation magnitude irrespective of direction.

All variables contributed equally to the acquisition-level summary metrics, and no normalization according to span length was performed. Both MADref and RMSref were retained as complementary measures. MADref reflects the average absolute magnitude of the deviation and is less influenced by isolated high values. In turn, RMSref gives greater weight to larger discrepancies and more strongly reflects the acquisition's overall deviation magnitude. The same rationale applies to RMSrep in repeatability assessment.

Because the dataset consisted exclusively of derived linear and angular variables, root mean square values were not computed from point clouds or Cartesian coordinates, but from the set of variable-specific deviations within each acquisition. Linear and angular root mean square values were calculated separately within their respective domains.

In the six-implant configuration, linear and angular measurements were additionally categorized by implant location. Measurements involving the six implant pairs common to both configurations were analyzed separately from those involving posterior-distal implant pair combinations to evaluate whether deviation magnitude varied by intra-arch region. In addition, to compare the two configurations on identical inter-implant geometry, MADref and RMSref were recalculated for each six-implant acquisition using only the six inter-implant pairs common to both configurations and compared with the corresponding four-implant metrics, so that both configurations were summarized over the same pairs and with the same metric definitions (restricted between-configuration comparison).

All statistical analyses and figures were produced in IBM SPSS Statistics (version 29.0; IBM Corp, Armonk, NY, USA); axis and panel titles of Figures 4, 5, and S1 to S3 were edited afterward without modifying the plotted data. Tests were two-sid-

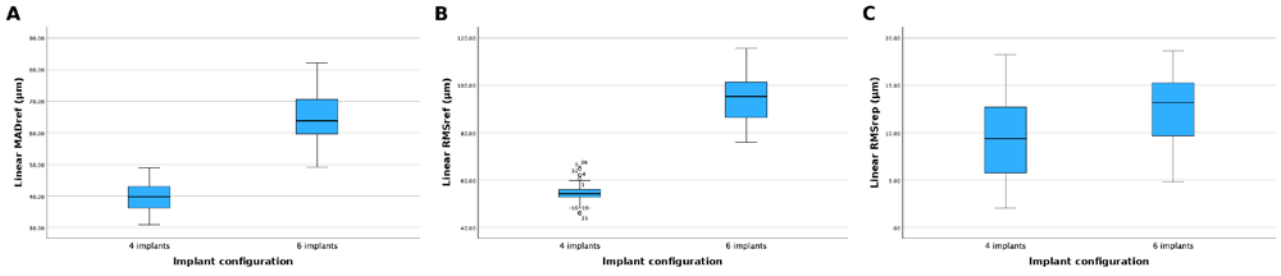


Figure 4. SPSS boxplots of acquisition-level linear metrics by implant configuration: reference-based deviation (A, mean absolute deviation from the reference values (MADref); B, root mean square deviation from the reference values (RMSref)) and repeatability (C, root mean square deviation from the operator-specific mean values (RMSrep)). Boxes show the interquartile range (IQR) with the median as a horizontal line; whiskers extend to the most extreme values within 1.5 × IQR of the box; circles indicate outliers (1.5 to 3 × IQR) and asterisks extreme values (more than 3 × IQR). Numbers next to these symbols are the case numbers of the corresponding acquisitions in the archived dataset. Vertical axes are expressed in micrometers (µm).

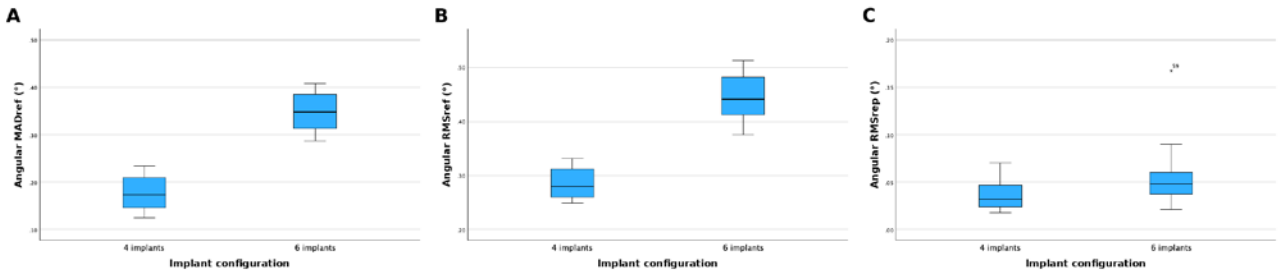


Figure 5. SPSS boxplots of acquisition-level angular metrics by implant configuration: reference-based deviation (A, mean absolute deviation from the reference values (MADref); B, root mean square deviation from the reference values (RMSref)) and repeatability (C, root mean square deviation from the operator-specific mean values (RMSrep)). Boxes show the interquartile range (IQR) with the median as a horizontal line; whiskers extend to the most extreme values within 1.5 × IQR of the box; circles indicate outliers (1.5 to 3 × IQR) and asterisks extreme values (more than 3 × IQR). Numbers next to these symbols are the case numbers of the corresponding acquisitions in the archived dataset. Vertical axes are expressed in degrees (°).

ed (α = 0.05), and data are reported as mean ± standard deviation. Configurations and operators were compared with independent-samples *t* tests (Welch's correction when Levene's test indicated unequal variances) and locations with paired-samples *t* tests, reporting mean differences, 95% confidence intervals (CIs), and Hedges' *g*. Non-normal angular metrics (Shapiro-Wilk test) were also analyzed with Mann-Whitney U and Wilcoxon signed-rank tests. Holm-Bonferroni adjustment was applied within the between-configuration (six unrestricted and four restricted comparisons), operator-stratified (12), and location-stratified (two) families. In the text, *P* values for these families are Holm-adjusted unless labeled as unadjusted, whereas Tables 2 to 5 report both; nonparametric, mixed-model, and drift *P* values are unadjusted. Reproducibility was quantified as the root mean square deviation of each acquisition from the pooled configuration grand mean. Drift was explored by Spearman correlation and least-squares regression of linear and angular RMSref on acquisition order within each operator/configuration sequence.

As a robustness analysis accounting for the clustering of pairwise measurements within acquisitions, linear mixed-effects models (REML; random intercept for acquisition) were fitted to the absolute pairwise deviations, with fixed effects for configuration, operator, and their interaction; location, operator, and their interaction within the six-implant configuration; and configuration, operator, their interaction, and inter-implant pair within the six common pairs. Inter-operator variance components for linear RMSref were estimated per configuration (REML) and expressed as a proportion of total variance.

Linear RMSref thresholds of 75, 100, and 150 µm were used as descriptive benchmarks, not as validated clinical limits: the 150 µm threshold follows the framework misfit and passivity literature,[20–22] and 75 and 100 µm are exploratory fractions of that value.

Results

A total of 80 TUPEL acquisitions were analyzed, including 40 acquisitions for the four-implant configuration and 40 for the six-implant configuration. Shapiro-Wilk tests revealed that linear metrics were normally distributed ($P > .05$), whereas angular metrics deviated from normality. Therefore, angular metrics were additionally analyzed with nonparametric tests (Mann-Whitney U and Wilcoxon signed-rank tests) as a sensitivity analysis to the *t* tests applied to all metrics.

Table 1. Descriptive acquisition-level reference-based performance of the TUPEL 3D Dental Implant Scanner by implant configuration.

Metric	4 implants, mean ± SD	6 implants, mean ± SD
Linear MADref (µm)	39.68 ± 4.48	64.71 ± 7.43
Linear RMSref (µm)	54.60 ± 4.68	94.69 ± 9.27
Linear RMSrep (µm)	9.39 ± 4.15	12.52 ± 3.62
Angular MADref (°)	0.179 ± 0.033	0.346 ± 0.038
Angular RMSref (°)	0.286 ± 0.028	0.446 ± 0.040
Angular RMSrep (°)	0.037 ± 0.015	0.053 ± 0.024

MADref, mean absolute deviation from the reference values; RMSref, root mean square deviation from the reference values; RMSrep, root mean square deviation from the operator-specific mean values; SD, standard deviation.

The first null hypothesis, stating that TUPEL performance would not differ between configurations, was rejected. When considering all measured pairs, the six-implant configuration showed significantly higher deviations than the four-implant setup across all linear reference-based metrics. Specifically, mean linear MADref and RMSref were approximately 63% and 73% higher, respectively (both $P < .001$), while linear RMSrep was also higher in the six-implant configuration (by approximately 33%; Holm-adjusted $P = .003$). Table 1 summarizes these results. Angular reference-based metrics followed the same pattern, with significantly higher MADref and RMSref values in the six-implant configuration (approximately 94% and 56% higher, respectively) when all measured pairs were considered (both $P < .001$). Table 2 summarizes the corresponding between-configuration comparisons. Following Holm-Bonferroni adjustment, all unrestricted between-configuration differences remained significant (adjusted $P \leq .003$).

Table 2. Comparison of acquisition-level reference-based deviation and repeatability metrics between the four-implant and six-implant configurations.

Metric	Mean difference (4 implants minus 6 implants)	95% CI	P-value, unadjusted / Holm-adjusted [a]	Hedges' g
Linear MADref (µm)	−25.03	−27.77 to −22.29	< .001 / < .001	−4.04
Linear RMSref (µm)	−40.09	−43.38 to −36.81	< .001 / < .001	−5.41
Linear RMSrep (µm)	−3.13	−4.86 to −1.39	< .001 / .003	−0.80
Angular MADref (°)	−0.167	−0.183 to −0.151	< .001 / < .001	−4.64
Angular RMSref (°)	−0.159	−0.175 to −0.144	< .001 / < .001	−4.57
Angular RMSrep (°)	−0.017	−0.026 to −0.007	< .001 / .003	−0.81

[a] Unadjusted *P* values from independent-samples *t* tests / Holm-Bonferroni-adjusted *P* values (between-configuration family, ten comparisons). The 95% CIs for linear MADref, linear RMSref, and angular RMSref are Welch-corrected, as Levene's test indicated unequal variances.
CI, confidence interval; MADref, mean absolute deviation from the reference values; RMSref, root mean square deviation from the reference values; RMSrep, root mean square deviation from the operator-specific mean values.

Table 3. Comparison of acquisition-level reference-based deviation and repeatability metrics between Operator A (calibrated torque, 10 N·cm) and Operator B (manual finger-tightening).

Metric	4 implants, mean ± SD		P-value, unadjusted / Holm-adjusted a	6 implants, mean ± SD		P-value, unadjusted / Holm-adjusted a
	Operator A	Operator B		Operator A	Operator B	
Linear MADref (µm)	40.14 ± 4.73	39.22 ± 4.28	.525 / 1.000	59.38 ± 4.57	70.05 ± 5.71	< .001 / < .001
Linear RMSref (µm)	54.19 ± 5.33	55.01 ± 4.02	.583 / 1.000	87.33 ± 5.55	102.06 ± 5.60	< .001 / < .001
Linear RMSrep (µm)	8.93 ± 3.48	9.86 ± 4.78	.488 / 1.000	12.41 ± 4.18	12.63 ± 3.07	.849 / 1.000
Angular MADref (°)	0.209 ± 0.014	0.148 ± 0.014	< .001 / < .001	0.379 ± 0.018	0.312 ± 0.015	< .001 / < .001
Angular RMSref (°)	0.311 ± 0.015	0.262 ± 0.009	< .001 / < .001	0.479 ± 0.022	0.412 ± 0.021	< .001 / < .001
Angular RMSrep (°)	0.034 ± 0.013	0.040 ± 0.017	.277 / 1.000	0.058 ± 0.029	0.049 ± 0.018	.238 / 1.000

[a] Unadjusted *P* values from independent-samples *t* tests / Holm-Bonferroni-adjusted *P* values (operator-stratified family, 12 comparisons). MADref, mean absolute deviation from the reference values; RMSref, root mean square deviation from the reference values; RMSrep, root mean square deviation from the operator-specific mean values; SD, standard deviation.

The second null hypothesis, stating that operator-related factors would not influence deviation magnitude, was partially rejected. No significant differences were observed between operators for linear RMSrep values. However, inter-operator differences were observed for reference-based metrics, particularly in the six-implant configuration. Table 3 presents detailed operator-stratified results. After Holm-Bonferroni adjustment, angular inter-operator differences remained significant in both configurations, whereas linear inter-operator differences remained significant only in the six-implant configuration. Furthermore, reproducibility deviation (root mean square deviation from the configuration grand mean) exceeded repeatability deviation (RMSrep) in both configurations. Reproducibility was larger in the six-implant configuration than in the four-implant configuration: 16.50 ± 4.94 µm (linear) and 0.071 ± 0.021° (angular) versus 12.25 ± 4.02 µm and 0.056 ± 0.016°, respectively.

The third null hypothesis, stating that measurement location would not influence deviation magnitude, was rejected. Within the six-implant configuration, posterior-distal variables showed significantly greater deviations than anterior-central variables in both linear and angular domains. These paired comparisons are summarized in Table 4 and illustrated by operator in Supplementary Figure S1. The Wilcoxon signed-rank test confirmed the location effect, with all 40 acquisitions showing greater posterior-distal than anterior-central deviations in both domains ($Z = -5.51$, $P < .001$). Following Holm-Bonferroni adjustment, this location effect remained statistically significant.

Nonparametric Mann-Whitney U tests of the angular metrics confirmed the unrestricted between-configuration differences in MADref, RMSref, and RMSrep (all $P < .001$) and the inter-operator differences in MADref and RMSref for both configurations (all exact $P < .001$). Conversely, the inter-operator differences in angular RMSrep were not significant (exact $P = .369$ and .174 for the four- and six-implant configurations, respectively). In the restricted comparison, no statistically significant between-configuration differences were detected in angular MADref or RMSref (Mann-Whitney U test, $P = .844$ and .379). No acquisition exceeded the 150-µm linear RMSref benchmark (Supplementary Table S1).

Because the four- and six-implant configurations did not share the same set of pairwise measurements, an additional comparison was performed restricted to the six inter-implant pairs common to both configurations (i.e., the anterior-central pairs), using identical metric definitions (Table 5). In this restricted comparison, no statistically significant between-configuration differences were detected in angular deviations or in linear RMSref, and linear MADref was only slightly higher in the six-implant configuration (by approximately 8%; Holm-adjusted $P = .038$). Thus, approximately 88% of the unrestricted between-configuration difference in linear MADref and 99% in angular MADref were attributable to the inclusion of posterior-distal pairs. The two configuration-specific ATOS reference datasets agreed closely on the six common pairs (mean absolute difference 1.32 µm, maximum 3.31 µm; 0.003°, maximum 0.006°). Taken together, these findings indicate that the greater deviation observed in the six-implant configuration is primarily attributable to the inclusion of posterior-distal measurement locations rather than to implant number per se.

Table 4. Comparison of acquisition-level linear and angular absolute deviations between anterior-central and posterior-distal measurement locations within the six-implant configuration.

Metric	Anterior-central, mean ± SD	Posterior-distal, mean ± SD	Mean paired difference	95% CI	P-value, unadjusted / Holm-adjusted a
Linear absolute deviation (µm)	42.82 ± 5.95	79.31 ± 10.67	36.49	33.09 to 39.90	< .001 / < .001
Angular absolute deviation (°)	0.181 ± 0.034	0.456 ± 0.045	0.275	0.265 to 0.285	< .001 / < .001

[a] Unadjusted *P* values from paired-samples *t* tests / Holm-Bonferroni-adjusted *P* values (location-stratified family, two comparisons). CI – confidence interval; SD – standard deviation.

Table 5. Acquisition-level reference-based deviation metrics calculated over the same six anterior-central inter-implant pairs (34–32, 34–42, 34–44, 32–42, 32–44, and 42–44) common to the four-implant and six-implant configurations, with identical metric definitions.

Metric	4 implants, mean ± SD	6 implants (common pairs), mean ± SD	Mean difference	95% CI	P-value, unadjusted [a]	P-value, Holm-adjusted [b]
Linear MADref (µm)	39.68 ± 4.48	42.82 ± 5.95	−3.13	−5.48 to −0.79	.010	.038
Linear RMSref (µm)	54.60 ± 4.68	57.09 ± 6.68	−2.49	−5.06 to 0.08	.057	.172
Angular MADref (°)	0.179 ± 0.033	0.181 ± 0.034	−0.002	−0.017 to 0.013	.759	.901
Angular RMSref (°)	0.286 ± 0.028	0.291 ± 0.027	−0.005	−0.017 to 0.008	.451	.901

[a] Independent-samples *t* test.
[b] Holm-Bonferroni adjustment within the between-configuration family (ten comparisons).
CI, confidence interval; MADref, mean absolute deviation from the reference values; RMSref, root mean square deviation from the reference values; SD, standard deviation.

Signed (non-absolute) pairwise deviations from the reference were predominantly positive (634 of 840 pairwise measurements, 75.5%; mean signed deviation +43.4 ± 73.7 µm), indicating a systematic directional component in addition to random variation. This positive linear offset was present in the common pairs of both configurations (mean signed deviation +16.3 ± 52.4 µm and +21.5 ± 53.4 µm for the four- and six-implant configurations, respectively) and in both operators. Signed angular deviations were predominantly negative (622 of 840 pairwise measurements, 74.0%; mean signed deviation −0.244 ± 0.328°).

Within-sequence drift was limited (Supplementary Figures S2 and S3; Supplementary Table S2). No progressive deterioration was observed within the four-implant sequences: for Operator A, linear RMSref decreased slightly and angular RMSref increased slightly (both unadjusted $P < .05$; approximately 0.02° across the 20 acquisitions); no drift was detected for Operator B. In the six-implant configuration, linear RMSref decreased across Operator B's sequence (unadjusted $P < .01$), a trend confined to the posterior-distal pairs, whereas no drift was detected for Operator A.

The pairwise-level mixed-effects models fitted to absolute deviations confirmed the acquisition-level findings while accounting for clustering within acquisitions. For linear deviations, implant configuration was a significant fixed effect ($F(1,836) = 27.68$, $P < .001$), whereas operator ($F(1,836) = 1.05$, $P = .306$) and the configuration-by-operator interaction ($F(1,836) = 1.48$, $P = .224$) were not. For angular deviations, configuration ($F(1,836) = 67.00$, $P < .001$) and operator ($F(1,836) = 9.72$, $P = .002$) were significant, whereas the interaction was not ($F(1,836) = 0.03$, $P = .873$). Within the six-implant configuration, location was the dominant fixed effect for both linear ($F(1,596) = 42.33$, $P < .001$) and angular deviations ($F(1,596) = 175.55$, $P < .001$); operator was significant for angular ($F(1,596) = 10.14$, $P = .002$) but not for linear deviations ($F(1,596) = 2.64$, $P = .105$), and the location-by-operator interaction was not significant in either domain (linear, $F(1,596) = 1.92$, $P = .166$; angular, $F(1,596) = 0.05$, $P = .827$). In the model restricted to the six common inter-implant pairs, configuration was significant for linear ($F(1,471) = 6.97$, $P = .009$) but not for angular deviations ($F(1,471) = 0.34$, $P = .561$), consistent with the acquisition-level restricted comparison.

The between-acquisition random-intercept variance was estimated at or near the lower (zero) boundary in all models except the restricted linear model, in which it accounted for approximately 5% of the total variance, indicating limited clustering of pairwise measurements within acquisitions beyond that explained by the fixed effects. When the random-intercept variance is estimated at this boundary, the models are equivalent to fixed-effects linear models of the pairwise deviations.

The inter-operator variance component for linear RMSref, estimated using a variance-components (REML) model, was negligible in the four-implant configuration (0 µm² inter-operator variance versus 21.9 µm² residual variance) but accounted for a substantial proportion of total variance in the six-implant configuration (106.9 µm² inter-operator variance versus 31.1 µm² residual variance; proportion of variance attributable to operator ≈ 0.78). Because this component was estimated from only two operators, it is highly imprecise (asymptotic standard error ≈ 153 µm²) and should be interpreted descriptively.

Figures 4 and 5 present boxplots of linear and angular reference-based metrics by implant configuration, respectively. Supplementary Figures S1–S3 illustrate location-based deviations and acquisition-order run charts.

Discussion

The present study demonstrated that the performance of the TUPEL photogrammetry system was influenced by implant configuration, operator-related factors, and intra-arch measurement location. When all measured pairs were considered, the six-implant configuration showed higher linear and angular deviations than the four-implant configuration. These differences were statistically significant across the acquisition-level metrics evaluated, leading to the rejection of the first null hypothesis. This pattern was consistent across both MADref and RMSref, indicating that the longer-span configuration was associated with a greater overall magnitude of linear and angular deviation in the unrestricted six-implant comparison. However, because the four- and six-implant configurations did not share the same set of pairwise measure-

ments, this unrestricted comparison alone cannot distinguish an effect of implant number from an effect of measurement location.

When the comparison was restricted to the six inter-implant pairs common to both configurations, the between-configuration difference almost disappeared: no statistically significant difference in angular deviations was detected, and linear MADref was only 3.13 µm higher in the six-implant configuration, whereas posterior-distal pairs within the six-implant configuration showed markedly greater deviations than the same common inter-implant pairs. This indicates that the greater deviation observed in the unrestricted six-implant comparison is primarily driven by the posterior-distal measurement locations rather than by implant number itself, and the present findings should be interpreted accordingly. This finding is consistent with previous reports indicating that complete-arch digital implant acquisition becomes increasingly challenging as span length and implant number increase.[4,11,23,24] Studies of intraoral scanning and photogrammetry have reported differences in complete-arch acquisition accuracy across devices and experimental workflows.[8,10,13,23]

Regarding operator influence, no linear metric in the four-implant configuration showed significant inter-operator differences, whereas angular MADref and RMSref exhibited significant differences. In the six-implant configuration, significant inter-operator differences were observed for linear reference-based deviation metrics (MADref and RMSref), with Operator B showing higher deviation values, but not for repeatability. Importantly, the direction of the inter-operator differences was not consistent across measurement domains. Although Operator B showed greater linear reference-based deviations in the six-implant configuration, Operator A showed greater angular reference-based deviations in both configurations. Therefore, the observed differences cannot be attributed specifically to operator experience or scan body tightening method. Operator identity was confounded with tightening protocol and acquisition order, as Operator A used calibrated tightening and completed all acquisitions before Operator B, who used manual tightening. Accordingly, the present findings do not support recommending calibrated tightening over manual tightening. Rather, operator- and protocol-related factors may influence different measurement domains differently, although the present experimental design cannot isolate their individual contributions. This interpretation is consistent with the broader literature, which suggests that system performance depends not only on operator-related factors but also on acquisition protocol, recognition workflow, scan body seating conditions, and downstream data processing strategies.[2,9,10,13,15]

Deviation magnitude was location-dependent, with significantly greater linear and angular deviations for posterior-distal implant pairs than for the six inter-implant pairs common to both configurations, indicating greater reference-based deviation in distal areas of complete-arch configurations. Accordingly, the third null hypothesis was rejected. Several factors may explain this pattern. Posterior implants are located at greater distances from the central acquisition area, which may increase the system's sensitivity to small positional and angular discrepancies.[8,13] In addition, the geometric configuration of distal implants, often characterized by wider inter-implant spacing and reduced cross-arch stabilization, may contribute to error amplification.[11,12] The location effect was consistent between operators in both measurement domains, as the location-by-operator interaction was not significant for either linear or angular absolute deviations, supporting the pooled presentation of the location analysis (Table 4). This finding may be clinically relevant, as posterior-distal spans are typically the most demanding regions in complete-arch implant prosthodontics, both geometrically and prosthetically. The greater deviations observed in these regions also align with previous studies linking increased span length and more distal implant relationships with reduced digital accuracy.[13]

The present results are broadly consistent with previous reports indicating that photogrammetry systems perform favorably in complete-arch implant acquisition workflows.[5,8,10,12,25–29] A prior study reported that photogrammetry outperformed intraoral scanning and conventional impressions in an in vitro complete-arch setting, while another investigation similarly demonstrated favorable outcomes for stereophotogrammetry compared with digital and conventional techniques.[2,27] Clinical studies have also supported the relevance of photogrammetry-based workflows.[28–30] Across laboratory studies and systematic reviews, reported deviations vary with study design, reference strategy, and the performance metrics applied.[8,15,26,31]

The present study also contributes to the discussion of how to summarize deviation in complete-arch implant acquisition. MADref and RMSref were intentionally reported because they provide complementary information. MADref reflects the average absolute magnitude of the deviation and is less influenced by isolated high values, whereas RMSref assigns greater weight to larger discrepancies.[19,23,32,33] In complete-arch contexts, this distinction is particularly relevant, as localized deviations in long-span measurements may be relevant to the clinical interpretation of measurement performance even when the average absolute deviation appears moderate.[13] For the same reason, RMSrep was retained as a repeatability metric because it summarizes within-operator variability across the full set of variables rather than relying on a single span or measurement.[23,27] This dual-metric approach is consistent with metrological principles distinguishing absolute and squared-error-based summaries, each capturing different aspects of measurement performance.[16,34]

The restricted comparison deserves specific consideration, as it isolates the effect of adding two distal implants on identical inter-implant geometry. With the additional distal scan bodies, angular deviation showed no statistically significant difference, whereas linear MADref was 3.13 µm higher, an order of magnitude lower than the location effect (36.49 µm). These results do not demonstrate improved acquisition of the anterior-central implants with the wider marker distribution, but the nonsignificant angular result should not be interpreted as evidence of equivalence. This small linear difference may reflect the accommodation of marker positions farther from the central acquisition area, differences of similar magnitude between the two ATOS reference datasets (up to 3.31 µm), or acquisition order, which the present design cannot separate.

A learning effect would favor the later four-implant acquisitions, whereas operator fatigue and accumulated seating cycles on the anterior scan bodies would penalize them. However, the run charts showed no progressive deterioration within the four-implant sequences, and the only unfavorable trend (approximately 0.02° in angular RMSref for Operator A) occurred in a domain where no statistically significant difference was detected between configurations. A recent study using a coordinate-measuring machine and separate four-, six-, and eight-implant casts reported that linear deviation increased and angular deviation decreased with implant number.[35] The present linear findings are directionally consistent, whereas no angular benefit was observed, possibly because of differences in reference standard, arch, model design, and photogrammetry system.

A key strength of the present study is the use of acquisition-level summaries as the primary inferential unit, minimizing the risk of pseudoreplication, together with pairwise-level mixed-effects models accounting for clustering within acquisitions. In addition, the use of a previously validated master model framework provides methodological continuity with prior investigations while allowing evaluation of a distinct acquisition system and outcome structure. The fact that all numerical analyses and the plotted data of all graphs can be generated directly in IBM SPSS Statistics supports the analytical workflow's transparency because it enables independent verification of the results using the archived dataset without relying on external tools.

This study has some limitations that should be considered when interpreting the findings. The reference and test datasets were generated using different acquisition and reconstruction workflows: the reference dataset was obtained using PEEK scan bodies followed by implant reconstruction in exocad, whereas the TUPEL acquisitions used manufacturer-specific metallic scan bodies and the TUPEL implant library. Although both workflows used the same implant analog geometry, neither approach directly measured implant position independently of the scan body and library-based reconstruction process. Therefore, the observed reference-based deviations may reflect differences between the two workflows in addition to deviations associated with the TUPEL acquisition workflow. Furthermore, because the reference dataset was obtained with an industrial optical scanning system rather than a coordinate-measuring machine or a certified nominal geometry, the reported metrics should be interpreted as deviations relative to the selected reference standard rather than as measurements of absolute trueness in the strict metrological sense.

The fact that different examiners measured the TUPEL and ATOS datasets in Geomagic Control X represents another limitation. Operator A, who performed the TUPEL measurements, had been trained in the standardized measurement protocol by Operator B, who performed the ATOS reference measurements. However, intra-examiner repeatability of the Geomagic measurement procedure was not formally assessed. Therefore, examiner-related variability during the Geomagic measurement procedure cannot be excluded. Moreover, any examiner-related differences in defining the reference circles would act as a constant offset and may have contributed, together with the scan body and library differences, to the directional component of the signed deviations.

Operator identity was confounded with previous photogrammetry experience, scan body tightening protocol, and acquisition order. Operator A used a calibrated tool, while Operator B used manual tightening. Operator A completed all acquisitions before Operator B, and each operator always acquired the six-implant configuration before the four-implant configuration. Consequently, the present experimental design cannot isolate the individual effects of operator experience, tightening protocol, and acquisition order. This limitation should therefore be considered when interpreting the observed inter-operator differences.

Furthermore, this study evaluated a single master model, implant system, and software version in a laboratory setting, which limits extrapolation to other systems and the intraoral environment. Ambient temperature was not recorded during the acquisition sessions; therefore, compliance with the manufacturer-specified operating temperature range could not be retrospectively verified.

Another limitation is the very large standardized effect sizes (Hedges' g) observed for several between-configuration contrasts, which reflect small standard deviations relative to the mean differences and should not be interpreted as an index of clinical relevance independent of the absolute magnitude of the deviations reported. Additionally, because RMSrep was calculated from the same 20 acquisitions per operator/configuration combination used to derive the reference-based metrics, RMSrep values across acquisitions are not fully statistically independent, which should be considered when interpreting the precision of the repeatability estimates. The predominance of positive signed pairwise deviations (75.5% of measurements) suggests a systematic directional component to the observed deviations, consistent with the reference-workflow and examiner-related limitations described above, rather than purely random measurement variation; signed angular deviations were likewise predominantly negative.

Finally, acquisitions followed a fixed order within a single session per operator, so order-related effects cannot be completely excluded. These limitations indicate the need for prospective, randomized, and adequately matched in vitro and in vivo investigations before broader clinical recommendations can be drawn.

Conclusions

Within the limitations of this in vitro study, no statistically significant inter-operator difference in repeatability was detected for the TUPEL 3D Dental Implant Scanner in complete-arch implant acquisition, although repeatability was lower in the six-implant configuration. When all measured pairs were considered, the four-implant configuration showed lower linear and angular reference-based deviations than the six-implant configuration. However, this difference was primarily attributable to measurement location rather than implant number itself. Posterior-distal implant relationships were associated with greater deviations, indicating that, in this model, the intra-arch location of the measured implant

pairs was more strongly associated with photogrammetric deviation than the number of implants, although operator, tightening protocol, and acquisition order were confounded.

Inter-operator differences were observed for selected reference-based deviation metrics and were not consistent across measurement domains. Overall, these findings support the potential of the evaluated photogrammetry system for complete-arch implant acquisition while highlighting the influence of intra-arch measurement location on reference-based deviation. Further independent investigations under clinical conditions are warranted to confirm these findings and determine their clinical relevance.

Conflict of interest

Duarte S. Marques is the Editor-in-Chief of the journal and was not involved in the editorial handling or peer review of this manuscript. The remaining authors declare no conflict of interest.

Ethical disclosures

Protection of human and animal subjects. The authors declare that no experiments were performed on humans or animals for this study.

Confidentiality of data. The authors declare that no patient data appear in this article.

Right to privacy and informed consent. The authors declare that no patient data appear in this article.

CRediT authorship contribution statement

Juliana L. Rainho: Conceptualization; Data curation; Formal analysis; Investigation; Visualization; Writing – original draft; Writing – review & editing. **Ricardo J. Pinto:** Data curation; Investigation; Methodology; Software. **Francisco J. Maligno da Silva:** Visualization; Writing – original draft; Writing – review & editing. **João M. Caramês:** Conceptualization; Methodology; Project administration; Resources; Supervision; Validation. **Duarte S. Marques:** Conceptualization; Formal analysis; Methodology; Project administration; Resources; Supervision; Validation; Visualization; Writing – review & editing.
All authors have read and agreed to the published version of the manuscript.

ORCID

Juliana Lima Rainho 0009-0001-1715-9160
Ricardo Jorge Marques Pinto 0000-0002-9710-5444
Francisco João Marques Maligno da Silva 0000-0003-1270-9597
João Manuel Mendez Caramês 0000-0002-5544-3744
Duarte Nuno Silva Marques 0000-0003-1966-8281

REFERENCES

1. Jemt T, Lie A. Accuracy of implant-supported prostheses in the edentulous jaw. Analysis of precision of fit between cast gold-alloy frameworks and master casts by means of a three-dimensional photogrammetric technique. Clin Oral Implants Res. 1995;6(3):172–80.
2. Tohme H, Lawand G, Chmielewska M, Makhzoume J. Comparison between stereophotogrammetric, digital, and conventional impression techniques in implant-supported fixed complete arch prostheses: an in vitro study. J Prosthet Dent. 2023;129(2):354–62.
3. Di Fiore A, Meneghello R, Graiff L, Savio G, Vigolo P, Monaco C, et al. Full arch digital scanning systems performances for implant-supported fixed dental prostheses: a comparative study of 8 intraoral scanners. J Prosthodont Res. 2019;63(4):396–403.
4. Pinto RJ, Casado SA, Chmielewski K, Caramês JM, Marques DS. Accuracy of different digital acquisition methods in complete arch implant-supported prostheses: an in vitro study. J Prosthet Dent. 2024;132(1):172–7.
5. Jain S, Daak HA, Someli LA, Alamer AY, Apratim A, Akoor RMA, et al. Accuracy of stereophotogrammetry technique versus intraoral scanners for complete-arch implant digital impressions: a systematic review and meta-analysis. Eur J Dent. 2026;20(1):34–48.
6. Goodacre CJ, Bernal G, Rungcharassaeng K, Kan JYK. Clinical complications with implants and implant prostheses. J Prosthet Dent. 2003;90(2):121–32.
7. Papaspyridakos P, Chen CJ, Chuang SK, Weber HP, Gallucci GO. A systematic review of biologic and technical complications with fixed implant rehabilitations for edentulous patients. Int J Oral Maxillofac Implants. 2012;27(1):102–10.
8. Abuduwaili K, Huang R, Song J, Liu Y, Chen Z, Huang B, et al. Comparison of photogrammetric imaging, intraoral scanning and conventional impression accuracy of full-arch dental implant rehabilitation: an in vitro study. BMC Oral Health. 2025;25(1):753.
9. Gómez-Polo M, Barmak AB, Ortega R, Rutkunas V, Kois JC, Revilla-León M. Accuracy, scanning time, and patient satisfaction of stereophotogrammetry systems for acquiring 3D dental implant positions: a systematic review. J Prosthodont. 2023;32(Suppl 2):208–24.
10. Mangano FG, Lerner H, Valle G, Biaggini F, Mangano C, Dybov A. Trueness of extraoral photogrammetry, intraoral photogrammetry and direct intraoral scanning in the full-arch digital implant impression: a comparative in vitro study. J Dent. 2026;165:106269.
11. Papaspyridakos P, De Souza A, Finkelman M, Sicilia E, Gotsis S, Chen YW, et al. Digital vs conventional full-arch implant impressions: a retrospective analysis of 36 edentulous jaws. J Prosthodont. 2023;32(4):325–30.
12. Cheng J, Zhang H, Liu H, Li J, Wang HL, Tao X. Accuracy of edentulous full-arch implant impression: an in vitro comparison between conventional impression, intraoral scan with and without splinting, and photogrammetry. Clin Oral Implants Res. 2024;35(5):560–72.
13. Orejas-Perez J, Gimenez-Gonzalez B, Ortiz-Collado I, Thuissard IJ, Santamaria-Laorden A. In vivo complete-arch implant digital impressions: comparison of the precision of three optical impression systems. Int J Environ Res Public Health. 2022;19(7):4300.
14. Revilla-León M, Gómez-Polo M, Drone M, Barmak AB, Kois JC, Alonso Pérez-Barquero J. Accuracy of complete arch implant scans recorded by using intraoral and extraoral photogrammetry systems. J Prosthet Dent. 2025;134(6):2508–14.

15. Pozzi A, Laureti A, Tawil I, Chow J, Azevedo L, Fehmer V, et al. Intra oral photogrammetry: trueness evaluation of novel technology for implant complete-arch digital impression in vitro. Clin Implant Dent Relat Res. 2025;27(3):e70049.
16. International Organization for Standardization. ISO 5725-1:2023. Accuracy (trueness and precision) of measurement methods and results — Part 1: General principles and definitions [Internet]. 2nd ed. Geneva: ISO; 2023 [cited 2026 Sep 29]. Available from: https://www.iso.org/standard/69418.html
17. Pinto RJ, Martins JNR, Navarro JM, Caramês JM, Marques DS. Accuracy of intraoral scanners and photogrammetry for full-arch implant-supported rehabilitations: an in vitro study. Rev Port Estomatol Med Dent Cir Maxilofac. 2026;67. Epub 2026 Sep 21.
18. Tupel Ltd. Implant Scanner by MK3: User Instructions [Internet]. Oxford: Tupel Ltd; 2025 Oct [cited 2026 Sep 29]. Available from: https://dental3d.com.au/wp-content/uploads/2025/10/User-Instructions-MK3.pdf
19. Sicilia E, Lagreca G, Papaspyridakos P, Finkelman M, Cobo J, Att W, et al. Effect of supramucosal height of a scan body and implant angulation on the accuracy of intraoral scanning: an in vitro study. J Prosthet Dent. 2024;131(6):1126–34.
20. Manzella C, Bignardi C, Burello V, Carossa S, Schierano G. Method to improve passive fit of frameworks on implant-supported prostheses: an in vitro study. J Prosthet Dent. 2016;116(1):52–8.
21. Abdelrehim A, Etajuri EA, Sulaiman E, Sofian H, Salleh NM. Magnitude of misfit threshold in implant-supported restorations: a systematic review. J Prosthet Dent. 2024;132(3):528–35.
22. Harfagar G, Solis S, Hernandez M, Fehmer V, Sailer I, Azevedo L. Trueness and passivity of digital and conventional implant impressions in edentulous jaws: a prospective clinical study. Clin Implant Dent Relat Res. 2025;27(2):e70022.
23. Faria JC, Sampaio-Fernandes MA, Oliveira SJ, Malheiro R, Sampaio-Fernandes JC, Figueiral MH. Trueness of implant positioning using intraoral scanning and dental photogrammetry for full-arch implant-supported rehabilitations: an in vitro study. Appl Sci (Basel). 2025;15(14):8016.
24. Alfaraj A, Alqudaihi F, Khurshid Z, Qadiri O, Lin WS. Comparative analyses of accuracy between digital and conventional impressions for complete-arch implant-supported fixed dental prostheses—a systematic review and meta-analysis. J Prosthodont. 2026;35(3):252–74.
25. Altalla H, Alhelou H, Karaduman F, Alawawda O, Bayindir F. Comparative accuracy of photogrammetry and intraoral scanners in recordings for complete arch implant-supported prostheses: a systematic review and meta-analysis. J Prosthet Dent. 2026;135(5):e60–70.
26. Pozzi A, Arcuri L, Carosi P, Laureti A, Londono J, Wang HL. Photogrammetry versus intraoral scanning in complete-arch digital implant impression: a systematic review and meta-analysis. Clin Implant Dent Relat Res. 2025;27(3):e70059.
27. Ma B, Yue X, Sun Y, Peng L, Geng W. Accuracy of photogrammetry, intraoral scanning, and conventional impression techniques for complete-arch implant rehabilitation: an in vitro comparative study. BMC Oral Health. 2021;21(1):636.
28. Pozzi A, Carosi P, Gallucci GO, Nagy K, Nardi A, Arcuri L. Accuracy of complete-arch digital implant impression with intraoral optical scanning and stereophotogrammetry: an in vivo prospective comparative study. Clin Oral Implants Res. 2023;34(10):1106–17.
29. Negreiros WM, Sun TC, Jain S, Finkelman M, Gallucci GO, Hamilton A. Precision of complete-arch digital implant scans using photogrammetry and intra-oral scanning. An in vivo cross-over study: complete-arch implant scans: photogrammetry vs IOS. J Dent. 2025;161:105928.
30. Estibalez-Recasens M, Serrano-Granger C, Santamaría-Laorden A, Andreu-Vázquez C, Orejas-Pérez J. Precision of stereophotogrammetry in complete arch implant recordings: a clinical study. J Prosthet Dent. 2025;133(5):1242–9.
31. Prasad S, Barmak AB, Revilla-León M. A systematic review and meta-analysis of the accuracy of complete arch implant scanning techniques performed extraorally: reverse impression and extraoral photogrammetry methods. Report of the Committee on Research in Fixed Prosthodontics of the American Academy of Fixed Prosthodontics. J Prosthet Dent. 2026;136(1):e79–101.
32. Sampaio-Fernandes MA, Pinto R, Almeida PR, Sampaio-Fernandes MM, Marques D, Figueiral MH. Trueness of extraoral digital impressions for full-arch implant impressions—in vitro study. Materials (Basel). 2024;17(12):2932.
33. Fu XJ, Cai ZZ, Shi JY, Qiao SC, Tonetti MS, Lai HC, et al. Accuracy of a novel intraoral photogrammetry technique for complete-arch implant impressions: an in vitro study. Clin Oral Implants Res. 2025;36(8):991–9.
34. Joint Committee for Guides in Metrology (JCGM). International vocabulary of metrology – Basic and general concepts and associated terms (VIM). 3rd ed. JCGM 200:2012. Sèvres: JCGM; 2012.
35. Robert N, Albert A, Bechet E, Lamy M. Influence of the number of implants on the accuracy of complete-arch impressions: in vitro comparison of photogrammetry and intraoral scanners using a coordinate measuring machine. J Dent. 2026;172:106723.

Desvio à referência e repetibilidade de um sistema fotogramétrico em arcada completa: estudo *in vitro*

RESUMO

Objetivos: Avaliar o desvio à referência e a repetibilidade de um sistema de fotogrametria (TUPEL 3D) na aquisição de implantes em arcada completa, assim como a influência do número de implantes, da localização e do operador.

Métodos: Utilizou-se um modelo mandibular edêntulo *in vitro* com duas configurações: seis implantes e quatro implantes, juntamente com pilares multiunit. Dois operadores realizaram 80 aquisições (20 por operador/configuração). Compararam-se medições lineares e angulares interimplantares com uma referência obtida por scanner industrial. Testes *t* compararam configurações, operadores e localizações; apresentam-se valores de *P* ajustados por Holm.

Resultados: Considerando todos os pares, a configuração de seis implantes apresentou desvios superiores (desvio quadrático médio linear: 94,69 ± 9,27 versus 54,60 ± 4,68 µm; $P < 0,001$). Nos seis pares comuns às duas configurações, não se detetaram diferenças angulares significativas ($P = 0,901$) e o desvio absoluto médio linear diferiu ligeiramente (seis versus quatro implantes: 42,82 ± 5,95 versus 39,68 ± 4,48 µm; $P = 0,038$). Os desvios posteriores-distais foram superiores ($P < 0,001$). O desvio de repetibilidade linear foi superior com seis implantes (12,52 ± 3,62 versus 9,39 ± 4,15 µm;

ARTICLE IN PRESS

P = 0,003). As diferenças entre operadores no desvio à referência foram inconsistentes entre domínios.

Conclusões: Não se detetaram diferenças estatisticamente significativas de repetibilidade entre operadores e a repetibilidade foi inferior com seis implantes. Os maiores desvios nesta configuração associaram-se sobretudo às localizações posteriores-distais, e não ao número de implantes. (Rev Port Estomatol Med Dent Cir Maxilofac. 2026;67(x):xxx-xxx)

© 2026 Sociedade Portuguesa de Estomatologia e Medicina Dentária. Publicado por SPEMD. Este é um artigo Open Access sob uma licença CC BY-NC-ND (http://creativecommons.org/licenses/by-nc-nd/4.0/).

Palavras-chave:
Desenho assistido por computador
Arcada dentária
Implantes dentários
Técnica de impressão dentária
Prótese dentária suportada por implantes
Imagem tridimensional
Fotogrametria
Reprodutibilidade dos resultados